NJC

PAPER

View Article Online
View Journal | View Issue

Cite this: *New J. Chem.*, 2019, **43**, 2471

Effects of pore surfaces on the electronic states of metal complexes formed on bipyridine periodic mesoporous organosilica†

Soichi Shirai,* Minoru Waki, Yoshifumi Maegawa, Yuri Yamada and Shinji Inagaki

Bipyridine periodic mesoporous organosilica (BPy-PMO) is a porous material in which the pore walls consist of silica frameworks bridged by 2,2′-bipyridine (bpy) functional groups, and is expected to be a novel platform for catalysts and photocatalysts. Metal complexes formed on the pore surfaces of BPy-PMO are under unusual environmental conditions that are entirely different from those in the bulk solids or in solution. To understand the effects of the unique structural features of the pore surfaces on the metal complexes, this study focused on the combination of BPy-PMO with Re(bpy)$(CO)_3$Cl (Re-BPy-PMO) and analyzed the metal-to-ligand charge transfer (MLCT) absorption band of this material. UV/vis and infrared analyses demonstrated that the Re-complex in Re-BPy-PMO interacts with water molecules adsorbed on the pore surfaces. Quantum chemical calculations suggest that the Re-complex also interacts with SiOH groups on the silica framework. Combined interactions are responsible for the unexpectedly short MLCT absorption wavelength of Re-BPy-PMO. This hypothetical mechanism is consistent with a red shift of the MLCT absorption following trimethylsilylation, which transforms SiOH groups to $SiOSiMe_3$ (TMS) groups and removes adsorbed water. Calculations also suggest that the TMS group is more electron-donating than the SiOH group. Therefore, the trimethylsilylation should result in a blue shift of the MLCT absorption with regard to the substituent effect, which is inconsistent with the experimental observations. Evidently, the effect of the removal of water and SiOH groups is sufficiently powerful to counteract the blue shift. Thus, the pore-surface features have a significant influence on the metal complex.

Received 13th December 2018,
Accepted 2nd January 2019

DOI: 10.1039/c8nj06277c

rsc.li/njc

1 Introduction

Periodic mesoporous organosilica (PMO) is a class of porous materials with a highly-ordered porous structure, uniform pore sizes of 2–30 nm and pore walls in which organic functional groups are homogeneously and densely integrated.[1–5] PMO is synthesized by the poly-condensation of an organosilane precursor having the formula R–$\{Si(OR')_3\}_x$ (R: organic bridging group, R′: Me, Et, i-Pr, *etc.* and $x \geq 2$) in the presence of a template surfactant.[6–8] Thus, various functionalities originating from R can be introduced on the pore walls.[9,10] By taking advantage of this feature, PMOs with organic ligands that enable metal complex formation on the pore surfaces have been synthesized.[11–13] These PMOs show promise as novel platforms for functional materials such as catalysts and photocatalysts, and the immobilization of homogeneous complexes on PMOs may allow separation from reaction solutions, for recovery and reuse.[14–21] Porous structures having high surface areas and large pores are also advantageous with regard to obtaining efficient catalytic reactions. In particular, a PMO incorporating 2,2′-bipyridine (BPy-PMO, Fig. 1),[13] which acts as a chelating ligand for a wide variety of metal ions (such as Ru, Ir, Re, Pd and Mo), has special potential for a wide variety of applications.[22–27]

The metal complexes formed on the pore surfaces of BPy-PMO are unusual in that they are discretely fixed by an array of bipyridine (bpy) groups without fully contacting one another, in contrast to the bulk solid. These complexes also have no interactions with solvent molecules, unlike those in solution. The silica framework of BPy-PMO, which is connected to the bpy groups through Si–C bonds, behaves as a huge substituent

Toyota Central R&D Laboratories, Inc., Nagakute, Aichi 480-1192, Japan. E-mail: shirai@mosk.tytlabs.co.jp

† Electronic supplementary information (ESI) available: Assessment on functional and basis set dependence in TDDFT calculation (Table S1); detailed results of the excited state calculations (Table S2); molecular orbitals of the models (Fig. S1); molecular structure of the BPy-PMO-pore-wall model (Fig. S2); cell parameters and Cartesian coordinates of the BPy-PMO-pore-wall model (Table S3); results of population analyses of the ground and MLCT excited states of Re(bpy)$(CO)_3$Cl (Table S4); molecular structure of ReBPH (Fig. S3). See DOI: 10.1039/c8nj06277c

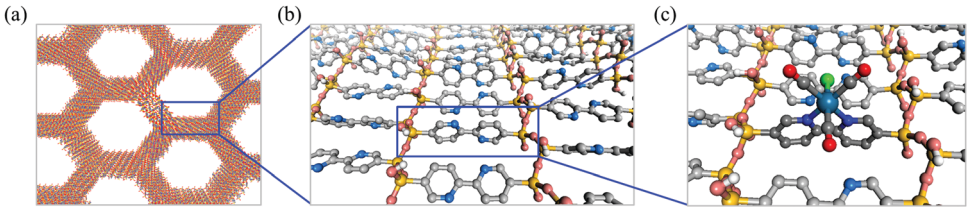

Fig. 1 Schematic images of (a) mesoporous structure of BPy-PMO, (b) molecular structure of pore-wall surface of BPy-PMO and (c) $Re(bpy)(CO)_3Cl$ formed on the BPy-PMO pore wall. The outermost layer of the pore wall is visualized in (b) and (c).

group and exhibits substituent effects on the complexes. In addition, silanol (SiOH) groups are densely distributed over the framework and thus are in close proximity to the complexes. These specific structural features have the potential to induce anomalous electronic properties in the metal complex, although the specific effects are still insufficiently understood.

In prior work, we formed $Re(bpy)(CO)_3Cl$ complexes on the bpy ligands embedded in the pore surfaces of BPy-PMO (Re-BPy-PMO) and investigated the physicochemical properties[26] and selective CO_2 reduction photocatalytic activity of the resulting materials.[28,29] This work found that the metal-to-ligand charge transfer (MLCT) absorption band (λ_{MLCT}) of Re-BPy-PMO in air is close to that of $Re(bpy)(CO)_3Cl$ in toluene. It has been reported that λ_{MLCT} is sensitive to both solvent polarity and the substituents on the bpy ligand, such that lower solvent polarity results in a longer λ_{MLCT}.[30–33] Thus, the λ_{MLCT} of Re-BPy-PMO in air should be longer than that of $Re(bpy)(CO)_3Cl$ in solution because air can be regarded as a solvent having an extremely low polarity ($\varepsilon_r \approx 1$). With regard to the substituent effect, λ_{MLCT} is red-/blue-shifted by electron-withdrawing/-donating substituents on the bpy ligand, and quantum chemical calculations suggest that a silica framework with SiOH groups behaves as an electron-withdrawing substituent.[34] Based on both these factors, the λ_{MLCT} of Re-BPy-PMO in air should be longer than that of $Re(bpy)(CO)_3Cl$ dissolved in any solution. However, actual experimental observations are inconsistent with this theoretical prediction. In fact, the environmental effects of the pore walls, which are derived from the unique structural features discussed above, most likely decide the experimentally-observed λ_{MLCT}. Assessing the MLCT absorption band of $Re(bpy)(CO)_3Cl$ formed on the pore surfaces enables a detailed investigation of environmental effects on the complex. Such information will definitely be useful in the future development of BPy-PMO-based functional materials.

In the present study, we examined the effects of the pore surfaces on a metal complex formed on BPy-PMO, focusing on the relationship between the λ_{MLCT} of $Re(bpy)(CO)_3Cl$ and the pore surface molecular structures. For this purpose, trimethylsilylated Re-BPy-PMO (Re-BPy-PMO-TMS), in which the SiOH groups have been converted to $SiOSiMe_3$ groups, was prepared and compared with the original Re-BPy-PMO to explore the factors affecting the λ_{MLCT}. Quantum chemical calculations were utilized to corroborate the mechanism proposed for the observed shifts of the λ_{MLCT}.

2 Experimental and computational details

2.1 Experiments

2.1.1 Materials. Re-BPy-PMO was synthesized according to a previously reported procedure.[13] BPy-PMO (50 mg) was added to a solution of $Re(CO)_5Cl$ (11.6 mg, 0.032 mmol) in toluene (10 mL) under an argon atmosphere. The suspension was stirred at 90 °C for 18 h, and filtered with toluene and CH_2Cl_2 to obtain Re-BPy-PMO. In this condition, the loading amount of the Re-complex should be 0.032 mmol at maximum, accounting for approximately 30% of the bpy units exposed on the pore surfaces. Re-BPy-PMO-TMS was synthesized by end-capping of the SiOH groups on the pore surfaces of Re-BPy-PMO using trimethylsilylimidazole in toluene at 60 °C.[22] Hereafter, this modification is referred to as trimethylsilylation.

2.1.2 Measurements. UV/vis diffuse reflectance spectra were acquired using a JASCO V-670 spectrometer with an integrating sphere unit following dilution of samples with $BaSO_4$ to avoid absorption saturation. Infrared (IR) spectra were acquired using a Thermo Fisher Scientific Nicolet Avatar-360 FT-IR spectrometer with an attenuated total reflection (ATR) attachment to confirm the presence of adsorbed water. IR spectra were also obtained after heating samples at 120 °C for 20 h under a reduced pressure of 70 Pa. *In situ* UV/vis spectra of each sample were acquired using a JASCO V-670 spectrometer with an integrating sphere unit and a vacuum chamber (the equipment used was different from the above). First, the spectrum in air was measured at ambient temperature, after which each sample was heated at 100 °C for 1 h under vacuum (less than 10 Pa) followed by cooling to ambient temperature. After the sample was allowed to stand for 20 min while maintaining the same reduced pressure, a second spectrum was recorded.

2.2 Calculations

Quantum chemical calculations were utilized to estimate λ_{MLCT} values and to explore the mechanism by which these values were shifted. All calculations were carried out utilizing the Gaussian09 program[35] and the following conditions were adopted unless otherwise noted. The molecular geometric structures were optimized using the density functional theory (DFT) method with the B3LYP functional[36,37] and the excited states were calculated using the time-dependent DFT (TDDFT) method[38–42] with the CAM-B3LYP functional.[43] The def2-TZVP and def2-SVP basis sets were employed for Re and for other elements, respectively.[44]

The functional and the basis sets for the TDDFT calculations were selected on the basis of our brief assessment (Table S1, ESI†). Single excitation from the second highest occupied molecular orbital (HOMO−1) to the lowest unoccupied molecular orbital (LUMO) is primarily responsible for the MLCT excitation of Re(bpy)$(CO)_3$Cl, giving an absorption band in the vicinity of 400 nm in the UV/vis spectrum.[30–32] The excited states corresponding to the HOMO−1 → LUMO excitation of Re(bpy)$(CO)_3$Cl were identified based on their dominant excitations and relevant molecular orbitals, and the calculated excitation energies were converted to wavelengths (nm) to obtain λ_{MLCT} values. Although spin–orbit interactions are typically significant in molecular systems with heavy atoms, it has been reported that, in the case of the λ_{MLCT} of Re(bpy)$(CO)_3$Cl, the values obtained by spin-free calculations are in good agreement with experimental results.[30–32] Thus, the spin-free TDDFT method was employed in this study.

2.2.1 Model complexes. Calculations were performed for Re(bpy)$(CO)_3$Cl, Re[5,5′-{Si$(OH)_3$}$_2$bpy]$(CO)_3$Cl and Re[5,5′-{Si$(OH)_2(OSiMe_3)$}$_2$bpy]$(CO)_3$Cl to estimate the substituent effect of the silica framework on λ_{MLCT}. Henceforth, Re[5,5′-{Si$(OH)_3$}$_2$bpy]$(CO)_3$Cl and Re[5,5′-{Si$(OH)_2(OSiMe_3)$}$_2$bpy]$(CO)_3$Cl are denoted as XOH and XOTMS, respectively. XOH is the simplest model of a Re-complex on BPy-PMO for which the bpy ligands are connected to the silica framework through Si–C bonds (Fig. 1(c)), and variation of the substituent effect following trimethylsilylation was examined by comparing XOH to XOTMS. In both cases, TDDFT calculations using the polarizable continuum model (PCM)[45–47] were also performed so as to examine the solvent effects of toluene, dichloromethane (CH_2Cl_2), acetonitrile (CH_3CN) and water (in ascending order of polarity). Re(bpy)$(CO)_3$Cl–$(H_2O)_n$ (n = 1, 2) clusters were additionally examined to investigate the interactions between Re(bpy)$(CO)_3$Cl and water molecules in more detail.

2.2.2 Pore-surface cluster models. Pore-surface cluster models were prepared utilizing first principles calculations. The pore walls of BPy-PMO were modeled as a periodic system with the unit cell consisting of SiO_3-bpy-Si_2O_3-bpy-Si ($C_{20}H_{12}N_4O_6Si_4$). The atomic positions, cell shape and volume were optimized using the DFT method with the optPBE-vdW functional.[48–52] The cutoff energy for the plane wave was set to 400 eV, a 3 × 6 × 6 gamma-centered Monkhorst–Pack k-point mesh[53] was used and Gaussian smearing with a width of 0.2 eV was applied. The convergence criterion for the optimization was set to 0.02 eV Å^{-1} of the forces on the nuclei. The calculations were performed using the VASP 5.4 program.[54,55] A supercell was created by repeating the optimized unit cell five times along the a and c axes, while two times along the b axis. Three bpy groups within the silica framework were cut out from the super cell along the c axis to prepare a BPy-PMO pore surface model, and the dangling bonds were saturated with OH groups. ReBP, the Re-BPy-PMO cluster model (Fig. 2(a)), was obtained by mounting Re$(CO)_3$Cl on the central bpy group, while ReBPT, a cluster model of Re-BPy-PMO-TMS (Fig. 2(b)), was prepared by converting six SiOH groups of ReBP (circled in Fig. 2(a)) to SiOSiMe_3 groups.

The molecular structures of ReBP and ReBPT were optimized and their excited states were calculated. The silica framework of the PMO forms a three-dimensional network structure, and both T^2 (R–Si(OH)$(OSi)_2$) and T^3 (R–Si$(OSi)_3$) species are present in large amounts in BPy-PMO synthesized under basic conditions,[13] suggesting that the silica framework of BPy-PMO is inflexible. Therefore, the positions of Si atoms were fixed for the duration of the optimizations of the cluster models, except for those in the OSiMe_3 groups of ReBPT.

3 Results and discussion

3.1 Experimental results

The UV/vis spectra acquired in this work are shown in Fig. 3. The λ_{MLCT} of Re-BPy-PMO had an absorption maximum at 403 nm, which is close to that of Re(bpy)$(CO)_3$Cl in toluene.[26] However, the λ_{MLCT} of Re-BPy-PMO-TMS was 416 nm, meaning that the trimethylsilylation of Re-BPy-PMO resulted in a red shift of the MLCT absorption.

The IR spectra are presented in Fig. 4. The Re-BPy-PMO spectrum exhibits an absorption peak around 1600 cm^{-1} that is assigned to the bending vibration of water.[56] This peak almost disappears upon heating under reduced pressure, indicating that the adsorbed water was almost completely removed. In the case of the Re-BPy-PMO-TMS, only a small peak was observed in

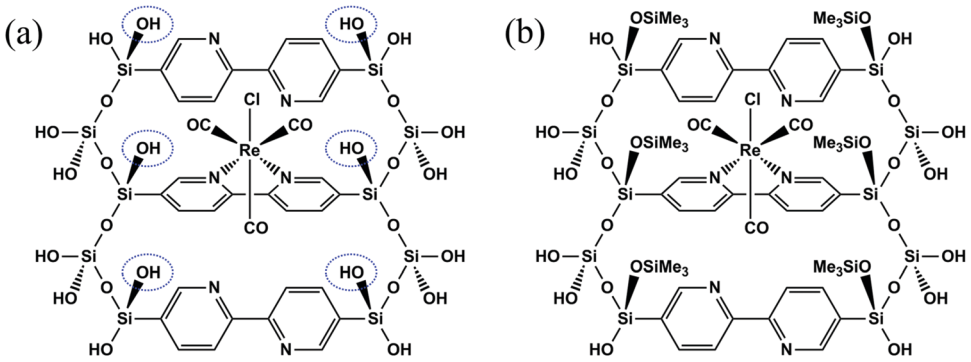

Fig. 2 Molecular structures of (a) ReBP and (b) ReBPT. ReBPT was prepared by converting circled OH groups of ReBP to OSiMe_3 groups.

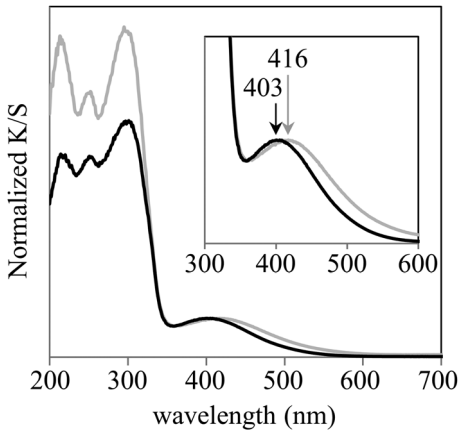

Fig. 3 UV/vis spectra of Re-BPy-PMO (black) and Re-BPy-PMO-TMS (gray).

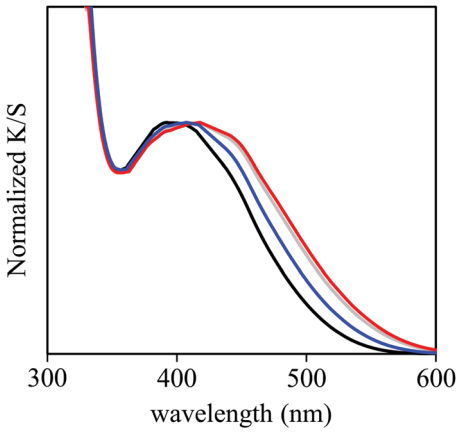

Fig. 5 *In situ* UV/vis spectra of Re-BPy-PMO before (black) and after (blue) vacuum heating; and Re-BPy-PMO-TMS before (gray) and after (red) vacuum heating. Detailed procedures are described in Section 2.1.2.

this region and the spectral change upon heating under reduced pressure was insignificant, suggesting that only a small amount of water was adsorbed on the pore surfaces. The lack of water is consistent with an increase in the hydrophobicity of the pore surfaces due to trimethylsilylation.

In the *in situ* UV/vis spectra, the MLCT absorption band of Re-BPy-PMO is red-shifted following the heating under vacuum and appears close to that generated by Re-BPy-PMO-TMS (Fig. 5). In contrast, the shift in the Re-BPy-PMO-TMS peak following the same treatment was negligible.

3.2 Calculation results

Vibrational analyses were carried out for the B3LYP-optimized geometries to confirm the absence of imaginary number frequencies. Because the second singlet excited state (S_2) of each model exhibited the largest oscillator strength in the wavelength region above 300 nm (Table S2, ESI†), this excited state was regarded as the origin of the visible MLCT absorption band. The HOMO−1 → LUMO single excitation was dominant in the S_2 states, while contributions from other excitations were negligible (Table S2, ESI†). Thus, these orbitals were carefully analyzed (Fig. S1, ESI†).

3.2.1 Model complexes and cluster models. The λ_{MLCT} wavelengths of model complexes calculated without PCM were in the order of XOH > XOTMS > Re(bpy)$(CO)_3$Cl and well correlated with the gaps between the HOMO−1 and LUMO energy levels, $\Delta_{H-1/L}$ (Table 1). Since the LUMO of Re(bpy)$(CO)_3$Cl is distributed over the bpy ligand (Fig. S1, ESI†), its energy level is greatly affected by the substituents on the ligand. In contrast, the HOMO−1 of Re(bpy)$(CO)_3$Cl is distributed over the Re$(CO)_3$Cl moiety and therefore only slightly affected by the ligand substituents. The LUMO level of XOH was lower than that of Re(bpy)$(CO)_3$Cl. The λ_{MLCT} wavelengths and the orbital levels confirm that $Si(OH)_3$ groups behave as electron-withdrawing groups, and so with silica frameworks of BPy-PMO. Meanwhile, the HOMO−1 and LUMO levels of XOTMS are higher than XOH, indicating that the $Si(OH)_2(OSiMe_3)$ group is more electron-donating than the $Si(OH)_3$ group. The LUMO rises more largely than HOMO−1, resulting in the larger $\Delta_{H-1/L}$ and the shorter λ_{MLCT} wavelength than XOH. The results predict that Re-BPy-PMO-TMS should have a shorter λ_{MLCT} wavelength than Re-BPy-PMO based on substituent effects, although the prediction is inconsistent with the experimental observations

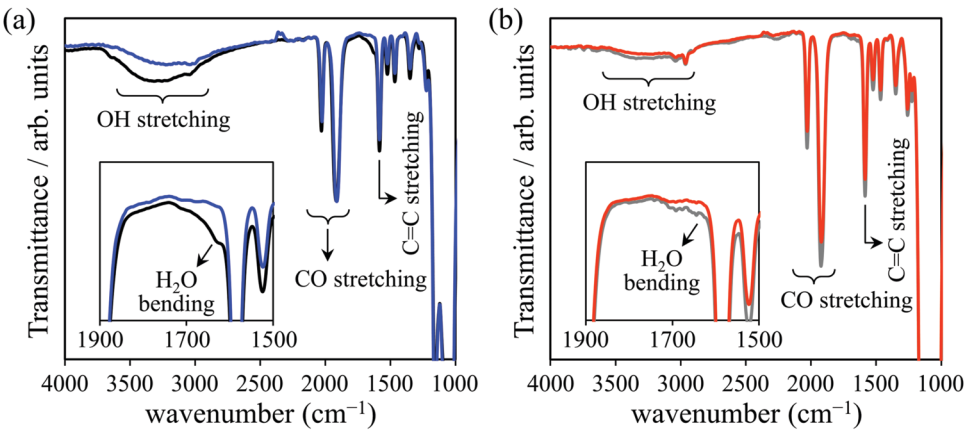

Fig. 4 IR spectra of (a) Re-BPy-PMO before (black) and after (blue) heating, and (b) Re-BPy-PMO-TMS before (gray) and after (red) heating.

Table 1 MLCT absorption wavelength (λ_{MLCT}), energy levels of HOMO−1 and LUMO, and their gaps ($\Delta_{H-1/L}$) calculated without PCM

Molecule	λ_{MLCT} (nm)	Orbital energy level (eV)		
		HOMO−1	LUMO	$\Delta_{H-1/L}$
Re(bpy)(CO)$_3$Cl	460.7	−6.85	−1.76	5.09
XOH[a]	471.0	−6.83	−1.85	4.98
XOTMS[b]	465.1	−6.80	−1.79	5.01
ReBP	404.7	−7.28	−1.82	5.46
ReBPT	432.8	−6.68	−1.46	5.22

[a] Re[5,5′-{Si(OH)$_3$}$_2$bpy](CO)$_3$Cl. [b] Re[5,5′-{Si(OH)$_2$(OSiMe$_3$)}$_2$bpy](CO)$_3$Cl.

in which the λ_{MLCT} of Re-BPy-PMO-TMS is longer than that of Re-BPy-PMO.

Fig. 6 and Fig. S2 show the 5 × 2 × 5 supercell created by replicating the optimized unit cell. The optimized cell parameters and the Cartesian coordinates of the atoms are provided in Table S3 (ESI†). The calculated length of the *c* axis (4.75 Å) is close to the intermolecular distance between the organic groups (4.4 Å), which was previously estimated by molecular mechanics calculations.[5] A cluster including three organic groups within the silica framework was cut out from this supercell along the *c* axis and was utilized to prepare the ReBP and ReBPT models (see Section 2.2.1).

The calculated λ_{MLCT} values of the model clusters are also collected in Table 1. The ReBP and ReBPT values were 404.7 and 432.8 nm, respectively, and thus were in good agreement with the experimental results, where the λ_{MLCT} values were in the order of Re-BPy-PMO < Re-BPy-PMO-TMS (Fig. 3). The HOMO−1 and LUMO levels of ReBPT were shifted upward by 0.60 and 0.36 eV from those of ReBP, leading to a smaller $\Delta_{H-1/L}$

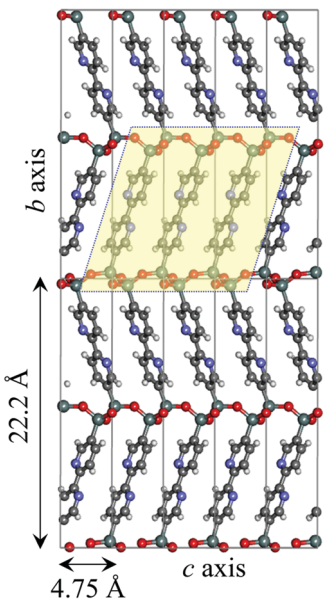

Fig. 6 Molecular structure of BPy-PMO pore-wall model optimized by utilizing first principle calculation. The *bc* plane of 5 × 2 × 5 supercell is presented. A cluster including three bipyridine groups and silica framework in a square were cut out and used for preparing ReBP and ReBPT (Fig. 2).

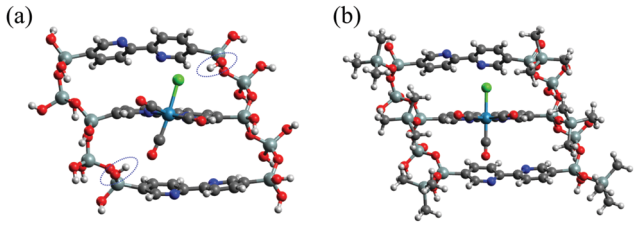

Fig. 7 Optimized structures of (a) ReBP and (b) ReBPT. OH groups interacting with the Re-complex moiety in ReBP are circled.

and a longer λ_{MLCT}. In this case, in contrast to the changes from XOH to XOTMS, the HOMO−1 level rises more significantly than the LUMO level. The optimized structures for ReBP and ReBPT are shown in Fig. 7. In ReBP, the OH bonds of SiOH groups are oriented relative to the CO and Cl ligands of the Re-complex moiety, suggesting hydrogen-bond-like interactions (Fig. 7(a)). These interactions attract the CO and Cl ligands to the SiOH groups and induce a slight distortion of the Re-complex. Such interactions and distortion of the complex are not observed in the case of the ReBPT, for which there are no SiOH groups around the complex.

3.2.2 Models with PCM and Re(bpy)(CO)$_3$Cl–(H$_2$O)$_n$. The calculated results for Re(bpy)(CO)$_3$Cl, XOH and XOTMS using the PCM approach are summarized in Table 2. A higher solvent polarity evidently resulted in a shorter λ_{MLCT}, and the calculated λ_{MLCT} values for Re(bpy)(CO)$_3$Cl are in good agreement with corresponding experimental values.[32] Although Re(bpy)(CO)$_3$Cl is poorly soluble in water, the estimated λ_{MLCT} in water was close to that in acetonitrile. Re(bpy)(CO)$_3$Cl in the ground state is polarized as Re(CO)$_3$Cl$^{\delta-}$–(bpy)$^{\delta+}$ because of the electron-withdrawing properties of the CO and Cl ligands, and the MLCT excitation results in reduced polarization.[57] For this reason, the ground state is stabilized by the solvent to a greater extent than the MLCT excited state and this effect is significant in a polar solvent. Calculated molecular orbital energy levels (Table 2),

Table 2 MLCT absorption wavelength (λ_{MLCT}), energy levels of HOMO−1 and LUMO, and their gaps ($\Delta_{H-1/L}$) calculated with PCM. Available experimental values are also presented

Molecule	Solvent	λ_{MLCT} (nm)		Orbital energy level (eV)		
		Calc.	Exptl.[a]	HOMO−1	LUMO	$\Delta_{H-1/L}$
Re(bpy)(CO)$_3$Cl	Toluene	408.9	403	−7.06	−1.59	5.47
	CH_2Cl_2	374.8	387	−7.24	−1.48	5.76
	CH_3CN	364.7	371	−7.31	−1.45	5.86
	Water	362.9		−7.32	−1.45	5.87
XOH[b]	Toluene	421.4		−7.08	−1.76	5.32
	CH_2Cl_2	389.1		−7.26	−1.69	5.57
	CH_3CN	379.5		−7.32	−1.67	5.66
	Water	377.7		−7.33	−1.66	5.67
XOTMS[c]	Toluene	417.8		−7.07	−1.72	5.35
	CH_2Cl_2	386.4		−7.26	−1.66	5.60
	CH_3CN	377.0		−7.32	−1.64	5.68
	Water	375.3		−7.33	−1.63	5.70

[a] Ref. 32. [b] Re[5,5′-{Si(OH)$_3$}$_2$bpy](CO)$_3$Cl. [c] Re[5,5′-{Si(OH)$_2$(OSiMe$_3$)}$_2$-bpy](CO)$_3$Cl.

populations and dipole moments (Table S4, ESI†) are consistent with this mechanism. The same mechanism is also applicable in the cases of the XOH and XOTMS, as suggested by the results in Table 2. The λ_{MLCT} values decreased in the order of XOH > XOTMS > Re(bpy)(CO)$_3$Cl regardless of the solvent, indicating that this order reflects substituent effects, so long as the solvent effects are equal.

The results for Re(bpy)(CO)$_3$Cl–(H$_2$O)$_n$ are collected in Table 3. The λ_{MLCT} was shortened with increases in n and the values were in the order of 1BPy > 1CO ≈ 1CL for n = 1 and 2BPy > 2CO ≈ 2CL for n = 2. These data demonstrate that the blue shift induced by the solvent primarily originates from the interactions of the solvent molecules with the CO and Cl ligands. The HOMO−1 levels of 1CO, 1CL, 2CO and 2CL were all shifted downward from those of Re(bpy)(CO)$_3$Cl, while the LUMO levels varied over a narrow range. The $\Delta_{H-1/L}$ value was therefore increased with increases in n and correlated with λ_{MLCT}. The optimized structures for Re(bpy)(CO)$_3$Cl–(H$_2$O)$_n$ are shown in Fig. 8. The O–H bonds of H$_2$O, which are polarized as $O^{\delta-}$–$H^{\delta+}$, are determined to be oriented relative to the CO and Cl ligands in 1CO, 1CL, 2CO and 2CL. The HOMO−1 of Re(bpy)(CO)$_3$Cl is stabilized when $H^{\delta+}$ approaches the CO and/or Cl ligands, since the orbital is distributed over the Re(CO)$_3$Cl moiety (Fig. S1, ESI†). Although the Re(bpy)(CO)$_3$Cl complex formed on BPy-PMO is half embedded in the pore wall, the CO and Cl ligands stick out from the pore surface and the space around these ligands is expected to be vacant. Therefore, the adsorbed water molecules can readily approach these ligands to induce a blue shift in the MLCT adsorption.

Table 3 Calculated MLCT absorption wavelengths (λ_{MLCT}), energy levels of HOMO−1 and LUMO, and their gaps ($\Delta_{H-1/L}$) in Re(bpy)(CO)$_3$Cl–(H$_2$O)$_n$. Optimized structures of the models are shown in Fig. 8

		Orbital energy level (eV)		
Model	λ_{MLCT} (nm)	HOMO−1	LUMO	$\Delta_{H-1/L}$
Re(bpy)(CO)$_3$Cl	460.7	−6.85	−1.76	5.09
1CO	423.9	−7.03	−1.69	5.34
1CL	421.3	−7.11	−1.77	5.34
1BPy	448.1	−6.69	−1.52	5.17
2CO	408.7	−7.05	−1.59	5.46
2CL	393.0	−7.35	−1.76	5.59
2BPy	434.0	−6.55	−1.29	5.26

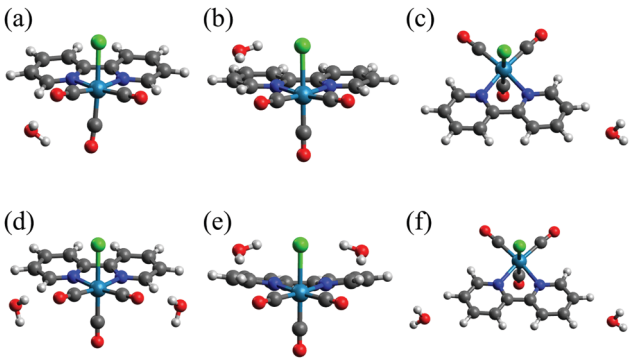

Fig. 8 Optimized structures of Re(bpy)(CO)$_3$Cl–(H$_2$O)$_n$: (a) 1CO, (b) 1CL, (c) 1BPy, (d) 2CO, (e) 2CL and (f) 2BPy.

In the optimized structures of 1BPy and 2BPy, water molecules interact with C–H bonds of the bpy ligand (Fig. 8(c and f)). In actual systems, the O–H bonds of water molecules may interact with π orbitals of the bpy ligand.[58] In our calculations of Re(bpy)(CO)$_3$Cl–(H$_2$O)$_n$, however, such structures were not obtained. In the calculation employing an initial structure of Re(bpy)(CO)$_3$Cl–(H$_2$O) in which a water molecule is placed above the bpy-ligand molecular plane, the water molecule departed from the bpy ligand and moved toward the CO or Cl ligands as a result of the geometry optimizations. The result suggests that the interactions of water molecules with the CO and Cl ligands are stronger than those with the bpy ligand. The O–H/π interactions may be predicted by incorporating the cluster of water molecules with hydrogen bond networks.

3.3 Discussion

The IR spectra (Fig. 4) suggest that water is adsorbed on the pore surfaces of Re-BPy-PMO in air, but is almost absent on Re-BPy-PMO-TMS. The interactions between the Re(bpy)(CO)$_3$Cl complex and water molecules induces a blue shift in the MLCT absorption band. This mechanism is supported by the red shift in the MLCT band of Re-BPy-PMO following heating under vacuum (Fig. 5) and the results of calculations incorporating solvent effects (Tables 2 and 3). Thus, it is likely that the blue shift due to adsorbed water dictates the experimentally-obtained ordering of the λ_{MLCT} values (Re-BPy-PMO < Re-BPy-PMO-TMS).

The optimized structure of ReBP shown in Fig. 7(a) suggests that the Re(bpy)(CO)$_3$Cl moieties of Re-BPy-PMO also interact with SiOH groups on the silica framework. The OH bonds of these SiOH groups are oriented relative to the CO and Cl ligands as well as the OH bonds of water molecules in Re(bpy)(CO)$_3$Cl–(H$_2$O)$_n$ (Fig. 8). The optimized structures suggest that the SiOH groups have similar effects to the water molecules and also contribute to a blue shift of the MLCT absorption band through the downward shift of the HOMO−1 level. To examine this hypothetical mechanism, ReBPH was prepared by substituting H atoms for the two OH groups that interact with the Re-complex moiety (Fig. S3, ESI†). The positions of these two H atoms were re-optimized and the λ_{MLCT} was calculated adopting the conditions described in Section 2.2. The resulting λ_{MLCT} of 446.1 nm was significantly longer than that for ReBP (404.7 nm). The HOMO−1 and LUMO levels of ReBPH were −6.79 and −1.64 eV, respectively, while the $\Delta_{H-1/L}$ was 5.15 eV (Table S2, ESI†). The reduced $\Delta_{H-1/L}$ is primarily attributed to the increase in the HOMO−1 level and is consistent with the change in λ_{MLCT}. The calculated λ_{MLCT} for ReBPH is longer even than that for ReBPT, which is consistent with the substituent effects of SiOH and SiOSiMe$_3$ groups estimated from the results for XOH and XOTMS (Table 1). As the predicted interactions between SiOH groups and Re(bpy)(CO)$_3$Cl moieties are originated from the local molecular structures around the Re-complex moieties, the calculation results are expected to be independent of the ReBP cluster size.

These results indicate that both adsorbed water and SiOH groups in Re-BPy-PMO induce a blue shift in the MLCT absorption band, resulting in the λ_{MLCT} values in the order of

Re-BPy-PMO < Re-BPy-PMO-TMS. The combined effects of the adsorbed water and SiOH groups are responsible for the unexpectedly short MLCT absorption wavelength of Re-BPy-PMO which is close to that of $Re(bpy)(CO)_3Cl$ in toluene.[26] The MLCT band of Re-BPy-PMO was red-shifted following heating in a vacuum, and its λ_{MLCT} approached that of Re-BPy-PMO-TMS (Fig. 5). The red shift can be attributed to the removal of adsorbed water, while the interactions between $Re(bpy)(CO)_3Cl$ moieties and SiOH groups remain even after the vacuum heating. The blue shift resulting from SiOH groups is responsible for the λ_{MLCT} of Re-BPy-PMO which is shorter than that of Re-BPy-PMO-TMS after the vacuum heating.

In the case of ReBP, the Re-complex moiety was distorted by the attractive interactions with SiOH groups (Fig. 7(a)). To examine the effect of this distortion on λ_{MLCT}, the complex moiety of ReBP was cut out from the optimized structure by breaking the Si–C bonds. The dangling bonds were terminated by H atoms and the positions of the two H atoms were re-optimized. The λ_{MLCT} was then calculated utilizing the same procedure and conditions discussed in Section 2.2. The calculated λ_{MLCT} was 461.4 nm (Table S2, ESI†) and thus similar to that of $Re(bpy)(CO)_3Cl$ having an optimized structure (460.7 nm, Table 1), indicating that the influence of the distortion was negligible.

The red shift of λ_{MLCT} following trimethylsilylation was inconsistent with the substituent effects suggested by the λ_{MLCT} values in the order of XOH > XOTMS (Table 1). The results demonstrate that the red shift due to the removal of the interactions of $Re(bpy)(CO)_3Cl$ moieties with the SiOH groups and adsorbed water counteracts the blue shift due to the change in the substituent effect. In this case, the structural properties of the pore surfaces have a significant influence on the electronic properties of the metal complex formed on the BPy-PMO. Thus, modification of the pore surfaces is a potential means of controlling the properties and functionalities of the metal complex, in addition to selecting specific metal ions and ligands. The effects of the modification of the pore surfaces on catalytic activity, selectivity and stability, as implied in our recent study,[27] are currently being investigated in our laboratory.

4 Conclusions

Metal complexes formed on the pore surfaces of BPy-PMO exist under unusual environmental conditions that are entirely different from those in the bulk solids or in solution. In this study, we examined the MLCT absorption band of $Re(bpy)(CO)_3Cl$ to understand the effects of the pore surfaces on the electronic properties of the complex. The experimental and calculation results indicate that the $Re(bpy)(CO)_3Cl$ moieties of Re-BPy-PMO interact with both adsorbed water and SiOH groups on the silica framework. These interactions contribute to a blue shift of the MLCT absorption band and are responsible for the significantly shorter λ_{MLCT} wavelength of Re-BPy-PMO which is close to that of $Re(bpy)(CO)_3Cl$ in toluene. These interactions are largely absent in Re-BPy-PMO-TMS, resulting in λ_{MLCT} values that increase in the order of Re-BPy-PMO < Re-BPy-PMO-TMS. The calculation results suggest that the $SiOSiMe_3$ group is more electron-donating than the SiOH group, and therefore trimethylsilylation contributes to a blue shift of the MLCT absorption with regard to the substituent effect. However, a red shift was experimentally observed following trimethylsilylation as a result of the removal of water molecules and SiOH groups, which was more powerful than the blue shift. Thus, the pore surface has dominant effects on the electronic properties of the metal complex.

Conflicts of interest

There are no conflicts to declare.

Acknowledgements

This work was partially supported by the Advanced Catalytic Transformation Program for Carbon Utilization (ACT-C) of the Japan Science and Technology Agency (JST) (Grant number: JPMJCR12Y1). Prof. Atsushi Satsuma at Nagoya University is acknowledged for his technical support while acquiring *in situ* UV/vis spectra. The authors are also grateful to Drs Ryoji Asahi and Nobuko Ohba at Toyota Central R&D Labs., Inc. for their suggestions, supports and encouragement.

References

1 S. Inagaki, S. Guan, Y. Fukushima, T. Ohsuna and O. Terasaki, *J. Am. Chem. Soc.*, 1999, **121**, 9611–9614.
2 T. Asefa, M. J. MacLachlan, N. Coombs and G. A. Ozin, *Nature*, 1999, **402**, 867–871.
3 B. J. Melde, B. T. Holland, C. F. Blanford and A. Stein, *Chem. Mater.*, 1999, **11**, 3302–3308.
4 C. Yoshina-Ishii, T. Asefa, N. Coombs, M. J. MacLachlan and G. A. Ozin, *Chem. Commun.*, 1999, 2539–2540.
5 S. Inagaki, S. Guan, T. Ohsuna and O. Terasaki, *Nature*, 2002, **416**, 304–307.
6 K. J. Shea, D. A. Loy and O. Webster, *J. Am. Chem. Soc.*, 1992, **114**, 6700–6710.
7 R. J. P. Corriu, *Angew. Chem., Int. Ed.*, 2000, **39**, 1376–1398.
8 D. A. Loy and K. J. Shea, *Chem. Rev.*, 1995, **95**, 1431–1442.
9 S. Fujita and S. Inagaki, *Chem. Mater.*, 2008, **20**, 891–908.
10 N. Mizoshita, T. Tani and S. Inagaki, *Chem. Soc. Rev.*, 2011, **40**, 789–800.
11 M. Waki, N. Mizoshita, T. Ohsuna, T. Tani and S. Inagaki, *Chem. Commun.*, 2010, **46**, 8163–8165.
12 M. Waki, N. Mizoshita, T. Tani and S. Inagaki, *Angew. Chem., Int. Ed.*, 2011, **50**, 11667–11671.
13 M. Waki, Y. Maegawa, K. Hara, Y. Goto, S. Shirai, Y. Yamada, N. Mizoshita, T. Tani, W. J. Chun, S. Muratsugu, M. Tada, A. Fukuoka and S. Inagaki, *J. Am. Chem. Soc.*, 2014, **136**, 4003–4011.
14 Z. M. Michalska and D. E. Webster, *Platinum Met. Rev.*, 1984, **18**, 65–73.

15 X. S. Zhao, X. Y. Bao, W. P. Guo and F. Y. Lee, *Mater. Today*, 2006, **9**, 32–39.
16 C. E. Song and S.-g. Lee, *Chem. Rev.*, 2002, **102**, 3495–3524.
17 D. E. De Vos, M. Dams, B. F. Sels and P. A. Jacobs, *Chem. Rev.*, 2002, **102**, 3615–3640.
18 P. McMorn and G. J. Hutchings, *Chem. Soc. Rev.*, 2004, **33**, 108–122.
19 C. Li, *Catal. Rev.: Sci. Eng.*, 2004, **46**, 419–492.
20 A. E. C. Collis and I. T. Horváth, *Catal. Sci. Technol.*, 2011, **1**, 912–919.
21 C. Perego and R. Millini, *Chem. Soc. Rev.*, 2013, **42**, 3956–3976.
22 Y. Maegawa and S. Inagaki, *Dalton Trans.*, 2015, **44**, 13007–13016.
23 X. Liu, Y. Maegawa, Y. Goto, K. Hara and S. Inagaki, *Angew. Chem., Int. Ed.*, 2016, **55**, 7943–7947.
24 N. Ishito, H. Kobayashi, K. Nakajima, Y. Maegawa, S. Inagaki, K. Hara and A. Fukuoka, *Chem. – Eur. J.*, 2015, **21**, 15564–15569.
25 Y. Kuramochi, M. Sekine, K. Kitamura, Y. Maegawa, Y. Goto, S. Shirai, S. Inagaki and H. Ishida, *Chem. – Eur. J.*, 2017, **23**, 10301–10309.
26 M. Waki, K.-i. Yamanaka, S. Shirai, Y. Maegawa, Y. Goto, Y. Yamada and S. Inagaki, *Chem. – Eur. J.*, 2018, **24**, 3846–3853.
27 S. Ishikawa, Y. Maegawa, M. Waki and S. Inagaki, *ACS Catal.*, 2018, **8**, 4160–4169.
28 J. Hawecker, J. M. Lehn and R. Ziessel, *J. Chem. Soc., Chem. Commun.*, 1983, 536–538.
29 J. Hawecker, J. M. Lehn and R. Ziessel, *Helv. Chim. Acta*, 1986, **69**, 1990–2012.
30 L. Yang, A. M. Ren, J. K. Feng, X. J. Liu, Y. G. Ma, M. Zhang, X. D. Liu, J. C. Shen and H. X. Zhang, *J. Phys. Chem. A*, 2004, **108**, 6797–6808.
31 A. Vlček and S. Zális, *J. Phys. Chem. A*, 2005, **109**, 2991–2992.
32 R. Heydová, E. Gindensperger, R. Romano, J. Sýkora, A. Vlček, S. Zális and C. Daniel, *J. Phys. Chem. A*, 2012, **116**, 11319–11329.
33 L. A. Worl, R. Duesing, P. Y. Chen, L. Dellaciana and T. J. Meyer, *J. Chem. Soc., Dalton Trans.*, 1991, 849–858.
34 S. Shirai, S. Iwata, Y. Maegawa, T. Tani and S. Inagaki, *J. Phys. Chem. A*, 2012, **116**, 10194–10202.
35 M. J. Frisch, G. W. Trucks, H. B. Schlegel, G. E. Scuseria, M. A. Robb, J. R. Cheeseman, G. Scalmani, V. Barone, G. A. Petersson, H. Nakatsuji, X. Li, M. Caricato, A. Marenich, J. Bloino, B. G. Janesko, R. Gomperts, B. Mennucci, H. P. Hratchian, J. V. Ortiz, A. F. Izmaylov, J. L. Sonnenberg, D. Williams-Young, F. Ding, F. Lipparini, F. Egidi, J. Goings, B. Peng, A. Petrone, T. Henderson, D. Ranasinghe, V. G. Zakrzewski, J. Gao, N. Rega, G. Zheng, W. Liang, M. Hada, M. Ehara, K. Toyota, R. Fukuda, J. Hasegawa, M. Ishida, T. Nakajima, Y. Honda, O. Kitao, H. Nakai, T. Vreven, K. Throssell, J. A. Montgomery, Jr., J. E. Peralta, F. Ogliaro, M. Bearpark, J. J. Heyd, E. Brothers, K. N. Kudin, V. N. Staroverov, T. Keith, R. Kobayashi, J. Normand, K. Raghavachari, A. Rendell, J. C. Burant, S. S. Iyengar, J. Tomasi, M. Cossi, J. M. Millam, M. Klene, C. Adamo, R. Cammi, J. W. Ochterski, R. L. Martin, K. Morokuma, O. Farkas, J. B. Foresman and D. J. Fox, *Gaussian 09, Revision D.01*, Gaussian, Inc., Wallingford CT, 2016.
36 A. D. Becke, *J. Chem. Phys.*, 1993, **98**, 5648–5652.
37 P. J. Stephens, F. J. Devlin, C. F. Chabalowski and M. J. Frisch, *J. Phys. Chem.*, 1994, **98**, 11623–11627.
38 E. Runge and E. K. U. Gross, *Phys. Rev. Lett.*, 1984, **52**, 997–1000.
39 E. K. U. Gross and W. Kohn, *Adv. Quantum Chem.*, 1990, **21**, 255–291.
40 C. Jamorski, M. E. Casida and D. R. Salahub, *J. Chem. Phys.*, 1996, **104**, 5134–5147.
41 M. Petersilka, U. J. Gossmann and E. K. U. Gross, *Phys. Rev. Lett.*, 1996, **76**, 1212–1215.
42 M. E. Casida, C. Jamorski, K. C. Casida and D. R. Salahub, *J. Chem. Phys.*, 1998, **108**, 4439–4449.
43 T. Yanai, D. P. Tew and N. C. Handy, *Chem. Phys. Lett.*, 2004, **393**, 51–57.
44 F. Weigend and R. Ahlrichs, *Phys. Chem. Chem. Phys.*, 2005, **7**, 3297–3305.
45 E. Cancès, B. Mennucci and J. Tomasi, *J. Chem. Phys.*, 1997, **107**, 3032–3041.
46 J. Tomasi, B. Mennucci and R. Cammi, *Chem. Rev.*, 2005, **105**, 2999–3093.
47 G. Scalmani and M. J. Frisch, *J. Chem. Phys.*, 2010, **132**, 114110.
48 J. Klimeš, D. R. Bowler and A. Michaelides, *J. Phys.: Condens. Matter*, 2010, **22**, 022201.
49 M. Dion, H. Rydberg, E. Schröder, D. C. Langreth and B. I. Lundqvist, *Phys. Rev. Lett.*, 2004, **92**, 246401.
50 M. Dion, H. Rydberg, E. Schröder, D. C. Langreth and B. I. Lundqvist, *Phys. Rev. Lett.*, 2005, **95**, 109902.
51 G. Román-Pérez and J. M. Soler, *Phys. Rev. Lett.*, 2009, **103**, 096102.
52 J. Klimeš, D. R. Bowler and A. Michaelides, *Phys. Rev. B: Condens. Matter Mater. Phys.*, 2011, **83**, 195131.
53 H. J. Monkhorst and J. D. Pack, *Phys. Rev. B: Solid State*, 1976, **13**, 5188–5192.
54 G. Kresse and J. Furthmüller, *Phys. Rev. B: Condens. Matter Mater. Phys.*, 1996, **54**, 11169–11186.
55 G. Kresse and J. Furthmüller, *Comput. Mater. Sci.*, 1996, **6**, 15–50.
56 D. B. Asay and S. H. Kim, *J. Phys. Chem. B*, 2005, **109**, 16760–16763.
57 K. A. Walters, Y. J. Kim and J. T. Hupp, *Inorg. Chem.*, 2002, **41**, 2909–2919.
58 L. V. Slipchenko and M. S. Gordon, *J. Phys. Chem. A*, 2009, **113**, 2092–2102.

